Multigrid Convergent Principal Curvature Estimators in Digital Geometry[1]

David Coeurjolly[a], Jacques-Olivier Lachaud[b,c], Jérémy Levallois[a,b,*]

[a] *Université de Lyon, CNRS, INSA-Lyon, LIRIS, UMR5205, F-69621, France*
[b] *Université de Savoie, CNRS, LAMA, UMR 5127, F-73776, France*
[c] *Université Grenoble-Alpes, CNRS, LJK, UMR 5224, F-38041, France*

Abstract

In many geometry processing applications, the estimation of differential geometric quantities such as curvature or normal vector field is an essential step. In this paper, we investigate a new class of estimators on digital shape boundaries based on Integral Invariants. More precisely, we provide both proofs of multigrid convergence of curvature estimators and a complete experimental evaluation of their performances.

Keywords: Digital geometry, curvature estimation, multigrid convergence, integral invariants.

1. Introduction

Context and objectives. In many shape processing applications, the estimation of differential quantities on the shape boundary is usually an important step. Their correct estimation makes easier further processing, like quantitative evaluation, feature detection, shape matching or visualization. This paper focuses on estimating the curvature tensor on the boundary of digital shapes. Such digital structures are subsets of the 3-dimensional digital space $\mathbb{Z}^3$ and come generally from the digitization of some Euclidean shape. Of course, the curvature tensor estimation should be as close as possible to the curvature tensor of the underlying Euclidean shape before digitization. Digital data form a special case of discrete data with specific properties: (1) digital data cannot sample the boundary of the Euclidean shape (i.e. they do not lie on the shape boundary), (2) digital data are distributed around the true sample according to arithmetic noise, which looks rather uniform over a range $[-h, h]$ from a statistical point of view, where h is the digitization grid step. Another way of stating these characteristics is to say that the Hausdorff distance between the Euclidean shape and its digitization is some $O(h)$. Of course, the quality of the estimation should be improved as the digitization step gets finer and finer. This property is called the *multigrid convergence* [1, 2]. It is similar in spirit with the *stability* property in Geometry processing: given a continuous shape and a specific sampling of if boundary, the estimated measure should converge to the Euclidean one when the sampling become denser (e.g. [3, 4]).

*Corresponding author.

Our objective is to design a curvature tensor estimator for digital data such that: (1) it is provably multigrid convergent, (2) it is accurate in practice, (3) it is computable in an exact manner, (4) it can be efficiently computed either locally or globally (evaluation at a single surface point or extraction of the curvature tensor field), (5) it is robust to further perturbations (like bad digitization around the boundary, outliers).

Related works for meshes. Digital data being discrete in nature, it is interesting to look at the curvature estimation techniques on triangulated meshes. In computer graphics and geometry processing, there exists a vast family of techniques to estimate curvatures, either only mean or gaussian curvature and sometimes the full curvature tensor. Most of them are local (i.e. limited to a 1-ring or 2-ring of neighbors) but exhibit correct results for nice meshes. They generally fall into three categories: fitting, discrete methods, curvature tensor estimation. We may refer to [5] and [6] for comprehensive evaluations, and Desbrun *et al.* [7] or Bobenko and Suris [8] for a more general theory. Most of them have not theoretical convergence guarantees even without noise on the mesh. We may quote [9] and [10] as approaches trying to tackle perturbation through averaging.

For Gaussian curvature estimated with Gauss-Bonnet approach (angle defect), Xu [11] provides a stability theorem for triangulated mesh whose vertices lie on the underlying smooth manifold, with valence 6 and parallelogram condition (each 1-ring of neighbors is projected as a parallelogram onto a plane). Assuming a sampling with density δ, he provides an additional convergence property whenever the sampling is perturbated by some $O(\delta^\alpha)$, but $\alpha > 2$ (inadequate for discrete data). Note that should the triangulated mesh not satisfy these requirements, then such estimation does not converge.

The integral measures of curvatures, based on normal cycle theory [12, 13] is another notable approach for estimating curvature information on a triangulated mesh. Authors exhibit some convergence results for triangulated meshes with vertices lying on the underlying smooth Euclidean shape boundary. In this case, if the mesh has Hausdorff distance to shape boundary below ϵ, convergence is obtained with speed/error $O(\epsilon)$ under some hypotheses.

Finally, in geometry processing, interesting mathematical tools have been developed to design differential estimators on smooth surfaces based on integral invariants [14, 15]. They consist in moving a kernel along the shape surface and in computing integrals on the intersection between the shape and the kernel. Authors have demonstrated that some integral quantities provide interesting curvature information when the kernel size tends to zero. They also achieve stability depending on the kernel radius and on ϵ, for instance in the case of a mesh sampling.

Related works for point clouds. When having only discrete data (i.e. a cloud of points), the most natural way to approach curvature(s) is to fit a polynomial surface of degree two at least. Perhaps the best representative of these techniques is the osculating jets of Cazals and Pouget [16]. The authors provide $O(\delta^2)$ convergence results in the case of where data is a surface sampling, assuming δ is the density of points.

There is no theoretical results in presence of noise, although the least-square fitting of osculating jets is very robust to noise in practice.

Another family of techniques exploit the voronoi diagram [17, 18, 4]. The idea behind these approaches is, instead of fitting the tangent space, to estimate at best the orthogonal space. The convolved covariance measure introduced by Mérigot *et al.* [4] is particularly appealing since this measure achieves robustness even for arbitrary compact sets, essentially in $O(\sqrt{\epsilon})$. It is in some sense an integral measure of the covariance matrix of the normal cone around the point of interest. However, convergence of curvature(s) is subject to several parameters r and R which contribute contradictorily to the Hausdorff error. In practice, this approach gives results comparable to osculating jets for curvatures.

Recently, several authors have developed new interesting approaches for estimating the normal vector field on noisy point of clouds, even in the presence of sharp features [19], [20], [21]. Furthermore, Boulch and Marlet [20] gives probabilistic convergence results. Although they cannot be used as is for curvature computation, they could be used in parallel with curvature estimation techniques to locate sharp features in a first pass, and to limit curvature estimations to smooth zones.

Related works for digital data. In Digital Geometry, we usually consider multigrid convergence as an essential criterion [2]. Hence, in dimension 2, parameter free convergence results have been obtained for length [22] and normal vector estimation [23]. Based either on binomial convolution principles [24, 25], or polynomial fitting [26], convergence results can also be obtained for higher order derivatives of digital curves. Algorithms are parametrized by the size of the convolution or fitting kernel support and convergence theorem holds when such support size is an increasing function of the grid resolution and some shape characteristics.

For curvature estimation along 2D curves, multigrid convergence of parameter free estimator is still challenging, although accurate experimental results have been obtained with maximal digital circular arcs [27] and with global optimization [28]. In 3D digital space, several empirical methods exist for estimating curvatures, but none achieves multigrid convergence (e.g. see [29, 30]). In [31], we recently presented a digital estimator for mean curvature for 2D and 3D digital objects, which achieve multigrid convergence in $O(h^{\frac{1}{3}})$.

Contributions. This paper completes [31] to propose a new curvature *tensor* estimator for digital data, which casts carefully the Integral Invariant (II) method of [14, 15] into the digital world. This estimator is a non-trivial extension of our mean digital curvature estimator [31], since it involves the compution of digital moments and covariance matrices, and requires results from matrix perturbation theory.

The contributions of the paper can be sketched as follows. First, we define digital versions of integral invariant estimators with multigrid convergence results (Theorems 3 and 4). We provide an explicit formula for the kernel size, which guarantees uniform convergence in $O(h^{\frac{1}{3}})$ for smooth enough curves and surfaces (Theorem 6). Furthermore, we demonstrate that these estimators have simple, exact and efficient implementations (available in DGtal library [32]). We provide an extensive comparative evaluation of these

estimators (mean curvature, principal curvatures), which shows that they compete with classical ones in terms of accuracy (Section 4). Computation speed is also considered, and our method is for instance ten times faster than the osculating jets. Finally, we show empirical results illustrating the robustness to noise and outliers of our estimators.

2. Preliminaries

2.1. Shapes, digital shapes and multigrid convergence

Since we are interested in evaluating both theoretically and experimentally the behavior of a given differential estimator on digital object boundaries, we first have to formalize links between Euclidean objects and digital ones with the help of a digitization process. Let us consider a family $\mathbb{X}$ of smooth and compact subsets of $\mathbb{R}^d$. In Section 2.3 we will be more precise on the notion of smoothness for shapes $X \in \mathbb{X}$. We denote $\mathtt{D}_h(X)$ the digitization of X in a $d-$dimensional grid of grid step h. More precisely, we consider classical Gauss digitization defined as

$$\mathtt{D}_h(X) \stackrel{def}{=} \left(\frac{1}{h} \cdot X\right) \cap \mathbb{Z}^d \tag{1}$$

where $\frac{1}{h} \cdot X$ is the uniform scaling of X by factor $\frac{1}{h}$. Furthermore, the set ∂X denotes the frontier of X (i.e. its topological boundary). If $z \in \mathbb{Z}^d$, then Q_z denotes the unit d-dimensional cube of $\mathbb{R}^d$ centered on z. The *h-frontier $\Delta_h Z$ of a digital set $Z \subset \mathbb{Z}^d$* is defined as $\Delta_h Z \stackrel{def}{=} \partial(h \cdot \cup_{z \in Z} Q_z)$. Therefore, the h-frontier of $\mathtt{D}_h(X)$ is a $d-1$-dimensional subset of $\mathbb{R}^d$, which is close to ∂X. We will precise the term "close" later in this section. Since this paper deals with multigrid convergence, digital shapes will always come from the digitization of continuous ones. To simplify notations, the h-frontier of the Gauss digitization at step h of a shape X will simply be denoted by $\partial_h X \stackrel{def}{=} \Delta_h \mathtt{D}_h(X)$, and called later on *$h$-boundary of X*.

As discussed in various previous works (see for instance [2] for a survey), the idea of multigrid convergence is that when we define a quantity estimator on $\mathtt{D}_h(X)$, we check if the estimated quantity converges (theoretically and/or experimentally) to the associated one on X when h tends to zero. More formally,

Definition 1 (Multigrid convergence for local geometric quantities). *A local discrete geometric estimator $\hat{E}$ of some geometric quantity E is* multigrid convergent *for the family $\mathbb{X}$ if and only if, for any $X \in \mathbb{X}$, there exists a grid step $h_X > 0$ such that the estimate $\hat{E}(\mathtt{D}_h(X), \hat{x}, h)$ is defined for all $\hat{x} \in \partial_h X$ with $0 < h < h_X$, and for any $x \in \partial X$,*

$$\forall \hat{x} \in \partial_h X \text{ with } \|\hat{x} - x\|_\infty \leq h, |\hat{E}(\mathtt{D}_h(X), \hat{x}, h) - E(X, x)| \leq \tau_{X,x}(h), \tag{2}$$

where $\tau_{X,x} : \mathbb{R}^+ \setminus \{0\} \to \mathbb{R}^+$ has null limit at 0. This function defines the speed of convergence of $\hat{E}$ toward E at point x of X. The convergence is uniform *for X when every $\tau_{X,x}$ is bounded from above by a function τ_X independent of $x \in \partial X$ with null limit at 0.*

When a geometrical quantity is global (*e.g.* area or volume), we do not need explicit mapping between ∂X and $\partial_h X$, and Definition 1 can be rephrased to define *multigrid convergence of global geometric quantities* [2]. A local discrete estimator thus estimates a geometric quantity at points on the h-frontier of a digital set, otherwise said at any point on the interpixel representation of the digital set boundary. This definition encompasses usual definitions where input points are pointels, linels or surfels.

In some proofs, a more precise mapping between points $x \in \partial X$ and $\hat{x} \in \partial_h X$ is required. For any shape $X \in \mathbb{R}^d$, the *medial axis* $\mathrm{MA}(\partial X)$ of ∂X is the subset of $\mathbb{R}^d$ whose points have more than one closest point to ∂X. The *reach* $\mathrm{reach}(X)$ of X is the infimum of the distance between ∂X and its medial axis. Shapes with positive reach have principal curvatures bounded by $\pm 1/\mathrm{reach}(X)$. The *projection* π^X is the mapping from $X \setminus \mathrm{MA}(\partial X)$ onto ∂X that associates to each point its closest point in ∂X (cf. Fig. 1-(*right*)).

This projection can be restricted to domain $\partial_h X$ in order to define a mapping π_h^X from the h-frontier $\partial_h X$ to the boundary ∂X. This mapping was called *back-projection* in [33]. For any 2D shape X with positive reach, for $0 < h \leq \mathrm{reach}(X)$, Lemma B.9 [33] indicates that the map π_h^X is well-defined and onto. It shows that the Hausdorff distance of boundaries $\partial_h X$ and ∂X is no greater than $\frac{\sqrt{2}}{2}h$, hence they get closer and closer as the grid step is refined.

In dD, it is possible to show[2] that their Hausdorff distance is no greater than $\frac{\sqrt{d}}{2}h$. Furthermore, it is a known fact that π^X is continuous over $\mathbb{R}^d \setminus \mathrm{MA}(\partial X)$, hence over $\partial_h X$ with an adequate h.

2.2. Integral invariants theory

In Geometry Processing, integral invariants have been widely investigated to define estimators of differential quantities (see [14, 15] for a complete overview). For short, the main idea is to move a kernel on points $x \in \partial X$ and to compute integrals on the intersection between X and the kernel. Even if different kernels (e.g., Euclidean ball, Euclidean sphere) and different integration functions can be considered, we focus here on volumetric integral invariants defined as follows:

Definition 2. *Given $X \in \mathbb{X}$ and a radius $r \in \mathbb{R}^{+*}$, the volumetric integral $V_R(x)$ at $x \in \partial X$ is given by (see Fig. 1−(left))*

$$V_R(x) \stackrel{def}{=} \int_{B_R(x)} \chi(p) dp \,, \tag{3}$$

where $B_R(x)$ is the Euclidean ball with radius R and center x and $\chi(p)$ the characteristic function of X. In dimension 2, we simply denote $A_R(x)$ such quantity.

Several authors have detailed connections between $V_R(x)$ and curvature (resp. mean curvature) at x for shapes in $\mathbb{R}^2$ (resp. $\mathbb{R}^3$) [34, 14, 15].

[2] The proof follows the same lines as Lemma B.9 [33].

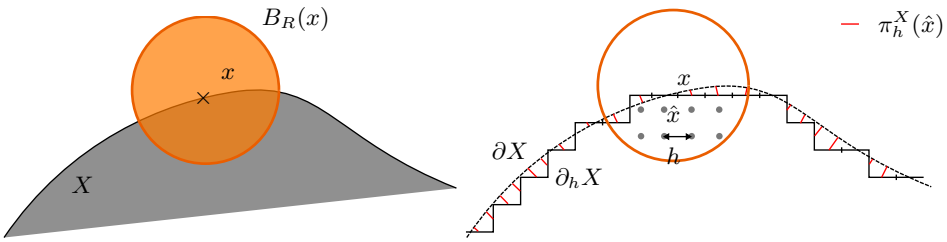

(a) (b)

Figure 1: Integral invariant computation (*left*) and notations (*right*) in dimension 2.

Lemma 1 ([15]). *For a sufficiently smooth shape X in $\mathbb{R}^2$, $x \in \partial X$, we have*

$$A_R(x) = \frac{\pi}{2}R^2 - \frac{\kappa(X,x)}{3}R^3 + O(R^4) \tag{4}$$

where $\kappa(X,x)$ is the curvature of ∂X at x. For a sufficiently smooth shape X in $\mathbb{R}^3$ and $x \in \partial X$, we have

$$V_R(x) = \frac{2\pi}{3}R^3 - \frac{\pi H(X,x)}{4}R^4 + O(R^5) \tag{5}$$

where $H(X,x)$ is the mean curvature of ∂X at x.

Such results are obtained by Taylor expansion at x of the surface ∂X approximated by a parametric function $y = f(x)$ in 2D and $z = f(x,y)$ in 3D. From Eq. (4) and (5) and with a fixed radius R, one can derive local estimators $\tilde{\kappa}_R$ and $\tilde{H}_R$ respectively:

$$\tilde{\kappa}_R(X,x) \stackrel{def}{=} \frac{3\pi}{2R} - \frac{3A_R(x)}{R^3}, \quad \tilde{H}_R(X,x) \stackrel{def}{=} \frac{8}{3R} - \frac{4V_R(x)}{\pi R^4} \tag{6}$$

In this way, when R tends to zero, both estimated values will converge to expected ones (respectively κ and H). More formally:

$$\tilde{\kappa}_R(X,x) = \kappa(X,x) + O(R), \quad \tilde{H}_R(X,x) = H(X,x) + O(R) \tag{7}$$

Similarly, directional information such as principal curvatures and thus Gaussian curvature can be retrieved from integral computations. Indeed, instead of computing the measure of $B_R(x) \cap X$ as in Def. 2, we consider its covariance matrix. Given a non-empty subset $Y \subset \mathbb{R}^d$, the *covariance matrix* of Y is given by

$$J(Y) \stackrel{def}{=} \int_Y (p - \overline{Y})(p - \overline{Y})^T dp = \int_Y pp^T dp - \mathrm{Vol}(Y)\overline{Y}\overline{Y}^T, \tag{8}$$

where $\overline{Y}$ is the *centroid* of Y and $\mathrm{Vol}(Y)$ its volume. For non negative integers p, q and s, we recall the definition of (p,q,s)-*moments* $m_{p,q,s}(Y)$ of Y:

$$m_{p,q,s}(Y) \stackrel{def}{=} \iiint_Y x^p y^q z^s dxdydz. \tag{9}$$

Note that the volume $\mathrm{Vol}(Y)$ is the 0-moment $m_{0,0,0}(Y)$, and that the centroid $\overline{Y}$ is the vector of 1-moments normalized by the 0-moment, i.e. $(m_{1,0,0}(Y), m_{0,1,0}(Y), m_{0,0,1}(Y))^T / m_{0,0,0}(Y)$. For simplicity, let us denote by A the Euclidean set $B_R(x) \cap X$. The covariance matrix of A is then rewritten as[3]:

$$J(A) = \begin{bmatrix} m_{2,0,0}(A) & m_{1,1,0}(A) & m_{1,0,1}(A) \\ m_{1,1,0}(A) & m_{0,2,0}(A) & m_{0,1,1}(A) \\ m_{1,0,1}(A) & m_{0,1,1}(A) & m_{0,0,2}(A) \end{bmatrix} - \frac{1}{m_{0,0,0}(A)} \begin{bmatrix} m_{1,0,0}(A) \\ m_{0,1,0}(A) \\ m_{0,0,1}(A) \end{bmatrix} \otimes \begin{bmatrix} m_{1,0,0}(A) \\ m_{0,1,0}(A) \\ m_{0,0,1}(A) \end{bmatrix}^T . \tag{10}$$

In [14], authors have demonstrated that eigenvalues and eigenvectors of $J(A)$ provide principal curvature and principal direction information:

Lemma 2 ([14], Theorem 2). *Given a shape $X \in \mathbb{X}$, the eigenvalues λ_1, λ_2, λ_3 of $J(A)$, where $A = B_R(x) \cap X$ and $x \in \partial X$, have the following Taylor expansion:*

$$\lambda_1 = \frac{2\pi}{15} R^5 - \frac{\pi}{48}(3\kappa^1(X,x) + \kappa^2(X,x))R^6 + O(R^7) \tag{11}$$

$$\lambda_2 = \frac{2\pi}{15} R^5 - \frac{\pi}{48}(\kappa^1(X,x) + 3\kappa^2(X,x))R^6 + O(R^7) \tag{12}$$

$$\lambda_3 = \frac{19\pi}{480} R^5 - \frac{9\pi}{512}(\kappa^1(X,x) + \kappa^2(X,x))R^6 + O(R^7) \tag{13}$$

where $\kappa^1(X,x)$ and $\kappa^2(X,x)$ denotes the principal curvatures of ∂X at x.[4]

Hence, similarly to Eq. (6), one can define local estimators $\tilde{\kappa}^1_R(X,x)$, $\tilde{\kappa}^2_R(X,x)$ and finally the Gaussian curvature $\tilde{K}_R(X,x) \overset{def}{=} \tilde{\kappa}^1_R(X,x) \cdot \tilde{\kappa}^2_R(X,x)$ as functions of $\{\lambda_i\}_{1,2,3}$ and R. From Lemma 2, all these estimators converge in the continuous setting when R tends to 0.

When dealing with digital shapes $\mathtt{D}_h(X)$, implementation of these estimators becomes straightforward: choose a radius R, center a Euclidean (or digital) ball at chosen points of $\partial_h X$ (e.g. centroids of linels or surfels), compute the quantities (area, volume, covariance matrix) and finally estimate curvature information $\tilde{\kappa}$, $\tilde{H}$, $\tilde{\kappa}^1$, $\tilde{\kappa}^2$ or $\tilde{K}$. However, several issues are hidden in this approach: What are meaningful values for R according to the shape size and geometry ? Do points of $\partial_h X$ converge to points $x \in \partial X$ for which Lemmas 1 and 2 are valid ? Does counting the number of pixels (resp. voxels) converge to $A_R(x)$ (resp. $V_R(x)$) ? Does the digital covariance matrix converges to the expected one ? The rest of the paper addresses all these questions.

[3] $\otimes$ denotes the usual tensor product in vector spaces.

[4] There is a typographic error in λ_1 in the paper [14].

2.3. Multigrid convergence of 2D and mean curvature estimator in digital space

In [31], we have demonstrated that digital versions of estimators defined in Eq. (6) leads to efficient and multigrid convergent estimators for 2D digital objects. In this section, we briefly describe the overall structure of this proof since similar arguments will be used in Sect. 3 to demonstrate that multigrid principal curvature digital estimators exist.

First, we used existing results on digital area or volume estimation by counting grid points. Hence, for $X \in \mathbb{X}$, we have

$$\begin{aligned} \widehat{\text{Area}}(\mathtt{D}_h(X), h) &\stackrel{def}{=} h^2 Card(\mathtt{D}_h(X)) = \text{Area}(X) + O(h^\beta), \\ \widehat{\text{Vol}}(\mathtt{D}_h(X'), h) &\stackrel{def}{=} h^3 Card(\mathtt{D}_h(X)) = \text{Vol}(X') + O(h^\gamma), \end{aligned} \tag{14}$$

for $\beta = \gamma = 1$ in the general case and $\beta = \gamma > 1$ with further constraints on $\mathbb{X}$ (*e.g.* C^3 with non-zero curvature) [35, 36, 37].

Then, we focused on the convergence of the area estimation on Euclidean shapes defined by $B_R(x) \cap X$ at $x \in \partial X$ in dimension 2. We defined a digital curvature estimator $\hat{\kappa}_R(\mathtt{D}_h(X), x, h)$ given from the area estimation by counting of $B_R(x) \cap X$ and Eq. (6), see [31], Eq. (11). We first demonstrated that $\hat{\kappa}_R(\mathtt{D}_h(X), x, h)$ converges to $\kappa(X, x)$ (note that curvatures are evaluated at the *same point* $x \in \partial X$):

Theorem 1 (Convergence of $\hat{\kappa}_R$ along ∂X, Theorem 1 of [31]). *Let X be some convex shape of $\mathbb{R}^2$, with at least C^2-boundary and bounded curvature. Then $\exists h_0, K_1, K_2$, such that*

$$\forall h < h_0, R = k_m h^{\alpha_m}, |\hat{\kappa}_R(\mathtt{D}_h(X), x, h) - \kappa(X, x)| \leq K h^{\alpha_m}, \tag{15}$$

where $\alpha_m = \frac{\beta}{2+\beta}, k_m = ((1+\beta)K_1/K_2)^{\frac{1}{2+\beta}}, K = K_2 k_m + 3K_1/k_m^{1+\beta}$. In the general case, $\alpha_m = \frac{1}{3}$.

Then, we showed that moving the digital estimation from $x \in \partial X$ to $\hat{x} \in \partial_h X$ does not change the convergence results:

Theorem 2 (Uniform convergence $\hat{\kappa}_R$ along $\partial_h X$, Theorem 2 of [31]). *Let X be some convex shape of $\mathbb{R}^2$, with at least C^3-boundary and bounded curvature. Then, $\exists h_0 \in \mathbb{R}^+$, for any $h \leq h_0$, setting $r = kh^{\frac{1}{3}}$, we have*

$$\forall x \in \partial X, \forall \hat{x} \in \partial_h X, \|\hat{x} - x\|_\infty \leq h \Rightarrow |\hat{\kappa}_R(\mathtt{D}_h(X), \hat{x}, h) - \kappa(X, x)| \leq K h^{\frac{1}{3}}.$$

In [31], we also presented similar results and convergence speed for mean curvature estimation in 3D from digital volume estimation.

To demonstrate that principal curvature estimators can be defined from digital version of integral invariants, we use the exact same process:

1. We first demonstrate that digital estimations of covariance matrix are multigrid convergent (Sect. 3.1 and 3.2);

2. Then, we give explicit error bounds on both the geometrical moments and the covariance matrix when we change the reference point from $x \in \partial X$ to $\hat{x} \in \partial_h X$ (Sect. 3.3 and 3.4) ;
3. Finally, we gather all these results to demonstrate that principal curvature estimators are uniformly multigrid convergent for all $\hat{x} \in \partial_h X$ (Sect. 3.5).

3. Multigrid convergence of principal curvature estimators in digital space

In this section, we derive digital principal curvature and principal direction estimators by digital approximation of those covariance matrices. Convergence results rely on the fact that digital moments converge in the same manner as volumes [37]. In the whole section, the considered family of shapes $\mathbb{X}$ is composed of compact subsets of $\mathbb{R}^3$ with positive reach, the boundary of which is C^3 and can be decomposed in a finite number of monotonous pieces. Compacity is required so that the boundary belongs to the shape. C^3-smoothness is required in the limited developments of Pottmann *et al.* [14, 15] relating covariance matrix and curvatures. Positive reach guarantees that two pieces of boundaries are not too close to each other, and this fact is also required in the previous limited developments (although this is not stated in their paper). The finite decomposition into monotonous pieces induces that integrals as limit of sums converge at speed at least $O(h)$.

3.1. Convergence of digital moments

Following the same principles as the area and volume estimators by counting, we define the *digital* (p, q, s)*-moments* $\hat{m}_{p,q,s}(Z, h)$ of a subset Z of $\mathbb{Z}^3$ at step h as

$$\hat{m}_{p,q,s}(Z, h) \stackrel{def}{=} h^{3+p+q+s} M_{p,q,s}(Z), \tag{16}$$

where $M_{p,q,s}(Z) \stackrel{def}{=} \sum_{(i,j,k)\in Z} i^p j^q k^s$. To shorten expressions, we denote by σ the sum $p+q+s$, which will always be an integer in $\{0, 1, 2\}$.

There exist multigrid convergent results for digital moments that are similar to the multigrid convergence of the area and the volume estimator (see Eq.(14)). Since their speed of convergence depends on the order σ of the moment, we may thus write for some constant $\mu_\sigma \geq 1$ [37]:

$$\hat{m}_{p,q,s}(\mathtt{D}_h(Y), h) = m_{p,q,s}(Y) + O(h^{\mu_\sigma}). \tag{17}$$

The involved constants μ_i are at least 1 in the general case, and some authors have established better bounds in places where the Gaussian curvature does not vanish (e.g. see [38] where $\mu_0 = \frac{38}{25} - \epsilon$, or [39], Theorem 1, where $\mu_0 = \frac{66}{43} - \epsilon$).

We wish to apply this formula to the set $A = B_R(x) \cap X$, whose size decreases with h. Big "O" notation in Eq. (17) hides the fact that the involved constant depend on the shape size, scale and maximal curvature. Hence, we need to normalize our moment estimation so that the error is no more influenced by the scale:

$$\begin{aligned}
\hat{m}_{p,q,s}(\mathtt{D}_h(A), h) &= h^{3+\sigma} M_{p,q,s}\left((\frac{1}{h} \cdot B_R(x) \cap X) \cap \mathbb{Z}^3 \right) \\
&= h^{3+\sigma} M_{p,q,s}\left(\frac{R}{h} \cdot (B_1(\frac{1}{R} \cdot x) \cap \frac{1}{R} \cdot X) \cap \mathbb{Z}^3 \right) \\
&= R^{3+\sigma} \left(\frac{h}{R}\right)^{3+\sigma} M_{p,q,s}\left(\mathtt{D}_{h/R}(B_1(\frac{1}{R} \cdot x) \cap \frac{1}{R} \cdot X) \right) \\
&= R^{3+\sigma} \hat{m}_{p,q,s}\left(\mathtt{D}_{h/R}(B_1(\frac{1}{R} \cdot x) \cap \frac{1}{R} \cdot X), \frac{h}{R} \right). \qquad (18)
\end{aligned}$$

The shape $B_1(\frac{1}{R} \cdot x) \cap \frac{1}{R} \cdot X$ tends toward a half-ball of radius 1 as R decreases. Therefore, we may apply Eq.(17) on Eq.(18) and consider that the involved constant does not depend on R or h. Note that we use below the obvious relation $m_{p,q,s}(R \cdot Y) = R^{3+\sigma} m_{p,q,s}(Y)$.

$$\begin{aligned}
\hat{m}_{p,q,s}(\mathtt{D}_h(A), h) &= R^{3+\sigma} \left(m_{p,q,s}\left(B_1(\frac{1}{R} \cdot x) \cap \frac{1}{R} \cdot X \right) + O\left(\frac{h}{R}\right)^{\mu_\sigma} \right) \\
&= m_{p,q,s}(B_R(x) \cap X) + O(R^{3+\sigma-\mu_\sigma} h^{\mu_\sigma}) \\
&= m_{p,q,s}(A) + O(R^{3+\sigma-\mu_\sigma} h^{\mu_\sigma}). \qquad (19)
\end{aligned}$$

Equation Eq.(19) is a multigrid convergent result for digital moments of subsets $B_R(x) \cap X$ valid for R decreasing as h decreases.

3.2. Digital approximation of covariance matrix around a point x

For any digital subset $Z \subset \mathbb{Z}^3$, we define its *digital covariance matrix* $\hat{J}(Z, h)$ *at step* h as:

$$\begin{aligned}
\hat{J}(Z,h) \stackrel{def}{=} & \begin{bmatrix} \hat{m}_{2,0,0}(Z,h) & \hat{m}_{1,1,0}(Z,h) & \hat{m}_{1,0,1}(Z,h) \\ \hat{m}_{1,1,0}(Z,h) & \hat{m}_{0,2,0}(Z,h) & \hat{m}_{0,1,1}(Z,h) \\ \hat{m}_{1,0,1}(Z,h) & \hat{m}_{0,1,1}(Z,h) & \hat{m}_{0,0,2}(Z,h) \end{bmatrix} \\
& - \frac{1}{\hat{m}_{0,0,0}(Z,h)} \begin{bmatrix} \hat{m}_{1,0,0}(Z,h) \\ \hat{m}_{0,1,0}(Z,h) \\ \hat{m}_{0,0,1}(Z,h) \end{bmatrix} \otimes \begin{bmatrix} \hat{m}_{1,0,0}(Z,h) \\ \hat{m}_{0,1,0}(Z,h) \\ \hat{m}_{0,0,1}(Z,h) \end{bmatrix}^T . \qquad (20)
\end{aligned}$$

We now establish the multigrid convergence of the digital covariance matrix toward the covariance matrix. In this case, we know the exact position of the point x at which both digital and continuous covariance matrices are computed. The following theorem only takes into account the integral approximation error.

Theorem 3 (Multigrid convergence of digital covariance matrix). *Let $X \in \mathbb{X}$. Then, there exists some constant h_X, such that for any grid step $0 < h < h_X$, for arbitrary $x \in \mathbb{R}^3$, for arbitrary $R \geq h$, with non-empty $A(R,x) \stackrel{def}{=} B_R(x) \cap X$, we have:*

$$\|\hat{J}(\mathtt{D}_h(A(R,x)), h) - J(A(R,x))\| \leq O(R^{5-\mu_0} h^{\mu_0}) + O(R^{5-\mu_1} h^{\mu_1}) + O(R^{5-\mu_2} h^{\mu_2}).$$

The constants hidden in the big O do not depend on the shape size or geometry. $\|\cdot\|$ *denotes the spectral norm on matrices.*

PROOF. To simplify expressions, we set $A \overset{def}{=} A(R,x)$, $A_h \overset{def}{=} \mathtt{D}_h(A(R,x))$. We begin by translating the sets A and A_h towards the origin w.r.t. x. We must use a vector that takes into account the digitization, hence we shift A_h by the vector $\left[\frac{x}{h}\right]$, the integer vector closest to $\frac{x}{h}$, and we shift A with the vector $h\left[\frac{x}{h}\right]$. We further set $\tilde{A}_h \overset{def}{=} \mathtt{D}_h(A) - \left[\frac{x}{h}\right]$ and $\tilde{A} \overset{def}{=} A - h\left[\frac{x}{h}\right]$. Following these definitions,

$$\hat{J}(\mathtt{D}_h(A(R,x)),h) = \hat{J}(A_h,h) = \hat{J}(\tilde{A}_h + \left[\frac{x}{h}\right],h)\,. \tag{21}$$

Using Lemma 4 (see Appendix A), we have

$$\hat{J}(\tilde{A}_h + \left[\frac{x}{h}\right],h) = \hat{J}(\tilde{A}_h,h)\,. \tag{22}$$

Writing down the definition of digital covariance matrix (see Eq.(20)), we have:

$$\begin{aligned}\hat{J}(\tilde{A}_h,h) = &\begin{bmatrix} \hat{m}_{2,0,0}(\tilde{A}_h,h) & & \\ & \ddots & \end{bmatrix} \\ &- \frac{1}{\hat{m}_{0,0,0}(\tilde{A}_h,h)} \begin{bmatrix} \hat{m}_{1,0,0}(\tilde{A}_h,h) \\ \vdots \end{bmatrix} \otimes \begin{bmatrix} \hat{m}_{1,0,0}(\tilde{A}_h,h) \\ \vdots \end{bmatrix}^T .\end{aligned} \tag{23}$$

We remark that $\tilde{A}_h = \mathtt{D}_h(A) - \left[\frac{x}{h}\right] = \mathtt{D}_h(A - h\left[\frac{x}{h}\right]) = \mathtt{D}_h(\tilde{A})$. Consequently, we apply convergence result of Eq.(19) onto set $\tilde{A}$ and insert them into Eq.(23) to get

$$\begin{aligned}\hat{J}(\tilde{A}_h,h) = &\begin{bmatrix} m_{2,0,0}(\tilde{A}) + O(R^{5-\mu_2}h^{\mu_2}) & & \\ & \ddots & \end{bmatrix} \\ &- \frac{1}{m_{0,0,0}(\tilde{A}) + O(R^{3-\mu_0}h^{\mu_0})} \begin{bmatrix} (m_{1,0,0}(\tilde{A}) + O(R^{4-\mu_1}h^{\mu_1}))^2 & & \\ & \ddots & \end{bmatrix} .\end{aligned} \tag{24}$$

Note that constants in big O are independent of X thanks to the normalization. In Eq.(24), we recognize easily $J(\tilde{A})$ plus other terms. We upper bound the other terms with two facts: (i) the radius R is greater than h, (ii) since $\tilde{A}$ is non-empty and close to the origin, we apply Eq.(A.2) and Eq.(A.4) of Lemma 5 for set $\tilde{A} \subset B_R(t)$ with $t = x - h\left[\frac{x}{h}\right]$, noticing that $\|t\|_\infty \leq \frac{h}{2}$. We obtain

$$\hat{J}(\tilde{A}_h,h) = J(\tilde{A}) + O(R^{5-\mu_2}h^{\mu_2}) + O(R^{5-\mu_0}h^{\mu_0}) + O(R^{5-\mu_1}h^{\mu_1}).$$

We conclude since $J(\tilde{A}) = J(A - h\left[\frac{x}{h}\right]) = J(A)$ by Lemma 4 (see Appendix A). □

3.3. Influence of a positioning error on moments

As for the mean curvature, We do not know generally the exact position of x but only some approximation $\hat{x}$ taken on the digital boundary $\partial_h X$. We therefore examine the perturbation of the moments when they are evaluated at a shifted position $x + \mathbf{t}$.

Lemma 3. *For any subset $X \subset \mathbb{R}^3$ and any vector $\mathbf{t}$ with norm $t \overset{def}{=} \|\mathbf{t}\|_2 \leq R$, we have for $0 \leq p+q+s \overset{def}{=} \sigma \leq 2$:*

$$m_{p,q,s}(B_R(x+\mathbf{t}) \cap X) = m_{p,q,s}(B_R(x) \cap X) + \sum_{i=0}^{\sigma} O(\|x\|^i t R^{2+\sigma-i}). \tag{25}$$

The proof is detailed in Appendix A.2.

3.4. Influence of a positioning error on covariance matrix

We now establish the multigrid convergence of the digital covariance matrix toward the covariance matrix even when the exact point x is unknown. We define

Theorem 4. (Multigrid convergence of digital covariance matrix with position error.) *Let $X \in \mathbb{X}$. Then, there exists some constant h_X, such that for any grid step $0 < h < h_X$, for arbitrary $R \geq h$, for any $x \in \partial X$ and any $\hat{x} \in \partial_h X$, $\|x - \hat{x}\|_\infty \leq h$, we have:*

$$\|\hat{J}(\mathtt{D}_h(A(R,\hat{x})), h) - J(A(R,x))\| \leq O(\|x-\hat{x}\|R^4) + \sum_{i=0}^{2} O(R^{5-\mu_i} h^{\mu_i}),$$

with $A(R,y) \overset{def}{=} B_R(y) \cap X$. The constants hidden in the big O do not depend on the shape size or geometry.

Proof. The fact that $\|x - \hat{x}\|_\infty \leq h \leq R$ induces that $A(R,x)$ and $A(R,\hat{x})$ are both non-empty. We cut the difference of two matrices into two parts:

$$\begin{aligned}\|\hat{J}(\mathtt{D}_h(A(R,\hat{x})), h) - J(A(R,x))\| \leq & \|\hat{J}(\mathtt{D}_h(A(R,\hat{x})), h) - J(A(R,\hat{x}))\| \\ & + \|J(A(R,\hat{x})) - J(A(R,x))\|.\end{aligned}$$

For the first error term, we apply directly Theorem 3 at point $\hat{x}$. For the second term, we set $\mathbf{t} \overset{def}{=} \hat{x} - x$, $t \overset{def}{=} \|\mathbf{t}\|$. Then we use the invariance of the covariance matrix with respect to translation to shift the problem toward the origin:

$$\begin{aligned}\|J(A(R,\hat{x})) - J(A(R,x))\| &= \|J(A(R,x+\mathbf{t})) - J(A(R,x))\| \\ &= \|J(A(R,x+\mathbf{t}) - x) - J(A(R,x) - x)\| \\ &= \|J((B_R(x+\mathbf{t}) - x) \cap (X - x)) - J((B_R(x) - x) \cap (X - x))\| \\ &= \|J(B_R(\mathbf{t}) \cap (X - x)) - J(B_R(0) \cap (X - x))\| \\ &= \|J(B_R(\mathbf{t}) \cap X') - J(B_R(0) \cap X')\|,\end{aligned}$$

with $X' \stackrel{def}{=} X - x$. We will apply Lemma 3 for the different moments in the covariance matrix J. We denote by Y_t the set $B_R(\mathbf{t}) \cap X'$ and by Y_0 the set $B_R(0) \cap X'$.

$$\|J(Y_t) - J(Y_0)\| = \left\| \begin{bmatrix} m_{2,0,0}(Y_t) - m_{2,0,0}(Y_0) & & \\ & \ddots & \end{bmatrix} - \frac{1}{m_{0,0,0}(Y_t)} \begin{bmatrix} m_{1,0,0}(Y_t) \\ \vdots \end{bmatrix} \otimes \begin{bmatrix} m_{1,0,0}(Y_t) \\ \vdots \end{bmatrix}^T + \frac{1}{m_{0,0,0}(Y_0)} \begin{bmatrix} m_{1,0,0}(Y_0) \\ \vdots \end{bmatrix} \otimes \begin{bmatrix} m_{1,0,0}(Y_0) \\ \vdots \end{bmatrix}^T \right\|.$$

Matrix $J(Y_t) - J(Y_0)$ contains order two geometrical moments difference (*e.g.* $m_{2,0,0}(Y_t) - m_{2,0,0}(Y_0)$) and quantities in the form of $\Delta \stackrel{def}{=} \frac{m_{1,0,0}(Y_t)^2}{m_{0,0,0}(Y_t)} - \frac{m_{1,0,0}(Y_0)^2}{m_{0,0,0}(Y_0)}$ (component $(1,1)$ in $J(Y_t) - J(Y_0)$ matrix). From Lemma 3, errors on second-order moments is in $O(tR^4)$. To bound Δ quantities, we first observe that $|m_{0,0,0}(Y_t) - m_{0,0,0}(Y_0)| = \pi R^2(t + O(t^2) + O(tR^2))$ using Theorem 7 in [15]. Hence,

$$\begin{aligned}
\Delta &= \frac{m_{1,0,0}(Y_t)^2}{m_{0,0,0}(Y_0) + O(tR^2)} - \frac{m_{1,0,0}(Y_0)^2}{m_{0,0,0}(Y_0)} \\
&= O(tR^2)\frac{m_{1,0,0}(Y_t)^2}{m_{0,0,0}(Y_0)^2} + \frac{m_{1,0,0}(Y_t)^2 - m_{1,0,0}(Y_0)^2}{m_{0,0,0}(Y_0)} && \left(\text{since } \frac{a}{b+O(x)} = \frac{a}{b} + \frac{a}{b^2}O(x)\right) \\
&= O(tR^4) + (m_{1,0,0}(Y_t) + m_{1,0,0}(Y_0))\frac{m_{1,0,0}(Y_t) - m_{1,0,0}(Y_0)}{m_{0,0,0}(Y_0)} && (\text{Lemma 3 and } a^2 - b^2 = (a-b)(a+b)) \\
&= O(tR^4) + (O(tR^3) + O(R^4))\frac{m_{1,0,0}(Y_t) - m_{1,0,0}(Y_0)}{m_{0,0,0}(Y_0)} && (\text{Lemma 5, Eq.(A.2)}) \\
&= O(tR^4) + (O(tR^3) + O(R^4))\frac{O(tR^3)}{m_{0,0,0}(Y_0)} && (\text{Lemma 3}) \\
&= O(tR^4) && (\text{since } t < R \text{ and } m_{0,0,0}(Y_0) = O(R^3)).
\end{aligned}$$

The same bound is found for all terms of the matrix. Putting everything together gives the result. □

3.5. Convergence for $\hat{x} \in \partial_h X$

Following the limited development of Lemma 2, we define estimators of curvatures from the diagonalization of the digital covariance matrix.

Definition 3. *Let Z be a digital shape, x some point of $\mathbb{R}^3$ and $h > 0$ a gridstep. For $R \geq h$, we define the* integral principal curvature estimators $\hat{\kappa}^1_R$ and $\hat{\kappa}^2_R$ *of Z at point $y \in \mathbb{R}^3$ and step h as*

$$\hat{\kappa}^1_R(Z, y, h) = \frac{6}{\pi R^6}(\hat{\lambda}_2 - 3\hat{\lambda}_1) + \frac{8}{5R}, \tag{26}$$

$$\hat{\kappa}^2_R(Z, y, h) = \frac{6}{\pi R^6}(\hat{\lambda}_1 - 3\hat{\lambda}_2) + \frac{8}{5R}, \tag{27}$$

where $\hat{\lambda}_1$ and $\hat{\lambda}_2$ are the two greatest eigenvalues of $\hat{J}(B_{R/h}(\frac{1}{h} \cdot y) \cap Z, h))$.

We recall the following result of matrix perturbation theory [40, 41]:

Theorem 5 (Lidskii-Weyl inequality). *If $\lambda_i(B)$ denotes the ordered eigenvalues of some symmetric matrix B and $\lambda_i(B+E)$ the ordered eigenvalues of some symmetric matrix $B+E$, then* $\max_i |\lambda_i(B) - \lambda_i(B+E)| \leq \|E\|$.

We prove below that our integral principal curvature estimators are multigrid convergent toward the principal curvatures along the shape.

Theorem 6. Uniform convergence of principal curvature estimators $\hat{\kappa}^1_R$ and $\hat{\kappa}^2_R$ along $\partial_h X$. *Let $X \in \mathbb{X}$. For $i \in \{1,2\}$, recall that $\kappa^i(X,x)$ is the i-th principal curvature of ∂X at boundary point x. Then, $\exists h_X \in \mathbb{R}^+$, for any $h \leq h_X$, setting $R = kh^{\frac{1}{3}}$, we have (for some positive constant k and K)*

$$\forall x \in \partial X, \forall \hat{x} \in \partial_h X, \|\hat{x} - x\|_\infty \leq h \Rightarrow |\hat{\kappa}^i_R(\mathtt{D}_h(X), \hat{x}, h) - \kappa^i(X,x)| \leq K h^{\frac{1}{3}}.$$

Proof. We prove the result for the first principal curvature, the proof for the second one is similar. According to Definition 3, $\hat{\lambda}_1$ and $\hat{\lambda}_2$ are the two greatest eigenvalues of $\hat{J}(B_{R/h}(\frac{1}{h}\cdot\hat{x}) \cap Z, h)$ with $Z = \mathtt{D}_h(X)$). We derive easily:

$$\begin{aligned}
\hat{J}(B_{R/h}(\frac{1}{h}\cdot\hat{x}) \cap \mathtt{D}_h(X), h) &= \hat{J}(B_{R/h}(\frac{1}{h}\cdot\hat{x}) \cap (\frac{1}{h}\cdot X) \cap \mathbb{Z}^3, h) \\
&= \hat{J}(\frac{1}{h}\cdot(B_R(\hat{x}) \cap X) \cap \mathbb{Z}^3, h) \\
&= \hat{J}(\mathtt{D}_h(B_R(\hat{x}) \cap X), h) \\
&= \hat{J}(\mathtt{D}_h(A(R,\hat{x})), h).
\end{aligned}$$

Theorem 4 indicates that $\hat{J}(\mathtt{D}_h(A(R,\hat{x})), h)$ and $J(A(R,x))$ are close to each other with a norm difference bounded by $O(\|x-\hat{x}\|R^4) + \sum_{i=0}^2 O(R^{5-\mu_i}h^{\mu_i})$. Since both matrices are symmetric by definition, Theorem 5 implies that $\hat{\lambda}_1$ and $\hat{\lambda}_2$ are close to the eigenvalues $\lambda_1(J(A(R,x)))$ and $\lambda_2(J(A(R,x)))$ with the same bound[5]. We thus write:

$$\begin{aligned}
\hat{\kappa}^1_R(\mathtt{D}_h(X), \hat{x}, h) &= \frac{6}{\pi R^6}(\hat{\lambda}_2 - 3\hat{\lambda}_1) + \frac{8}{5R} \\
&= \frac{6}{\pi R^6}\left(\lambda_2 - 3\lambda_1 + O(\|x-\hat{x}\|R^4) + \sum_{i=0}^2 O(R^{5-\mu_i}h^{\mu_i})\right) + \frac{8}{5R}.
\end{aligned}$$

We then substitute the limited development of Lemma 2 into the latter equation and we bound $\|x-\hat{x}\|$ by h. After some calculations, we get:

$$\hat{\kappa}^1_R(\mathtt{D}_h(X), \hat{x}, h) = \kappa^1(X,x) + O(R) + O(h/R^2) + \sum_{i=0}^2 O(h^{\mu_i}/R^{1+\mu_i}). \tag{28}$$

[5]Note that since error bounds tend to zero as h tends to zero, the ordering of the eigenvalues in both matrices is the same for a sufficiently small h.

Setting $R = kh^\alpha$, we optimize the value α to minimize all errors. Since $\mu_i \geq 1$ for the shape X, the optimal value is $\alpha = \frac{1}{3}$. The bound follows. □

It is worthy to note that the preceding error bound could be improved at neighborhoods where the gaussian curvature does not vanish: the constants μ_i are then closer to 1.5. However, there is the issue of estimating more precisely the position of $\hat{x}$ with respect to x. In the best known case, uniform convergence with bound $\approx O(h^{0.434})$ can be expected for radius R with a size proportional to $h^{0.434}$.

In Theorem 6, we focused on multigrid convergence of principal curvature quantities. However, similar results can be obtained for principal curvature directions as well.

4. Experimental evaluation

We present an experimental evaluation of curvature estimators in 2D and 3D. We have implemented these Integeral Invariant estimators (II) in the `DGtal` library [32] which allows us to have parametric or implicit shape construction in dimension 2 and 3 for multigrid evaluation. Furthermore, it allows comparison with former approaches available in `DGtal`: Most-centered Maximal Segment (MDSS), Most-centered Digital Circular Arc (MDCA) [27] and Binomial based convolution [25]. We also use `CGal` library in order to compare with *citer Monge via jet fitting* who provide a multigrid convergeant 3d estimator.

As a remember, we firstly need to construct a kernel from a Euclidean ball in dD with radius given by $R = k_m h^{\alpha_m}$ as described in theorem statements. Then, we track the digital object boundary, center the kernel on each surface elements and compute the intersection between the kernel and the object. For estimate 2d or 3d mean curvature, we compute the volume from this intersection; for 3d Gaussian curvature, we compute moments of the intersection in order to extract the eigenvalues from the covariance matrix using them.

Using this approach, we obtain a computational cost in $O((R/h)^d)$ per surface element (*i.e.* the size of the kernel digitization with grid-step h). However, we can take benefit from digital surface structure to considerably speed-up this algorithm: if we consider a surface tracker for which surface elements are processed by proximity (the current surface element is a neighbor of the previous one through a translation vector $\vec{\delta}$), the area/volume computation can be done incrementally since they are countable additive:

$$\begin{aligned}\widehat{\mathrm{Area}}(\mathtt{D}_h(X) \cap B_R(x+\vec{\delta}), h) &= \widehat{\mathrm{Area}}(\mathtt{D}_h(X) \cap B_R(x), h) \\ &+ \widehat{\mathrm{Area}}(\mathtt{D}_h(X) \cap (B_R(x+\vec{\delta}) \setminus B_R(x)), h) - \widehat{\mathrm{Area}}(\mathtt{D}_h(X) \cap (B_R(x) \setminus B_R(x+\vec{\delta})), h).\end{aligned}$$

On the same manner, with moments:

$$\begin{aligned}\hat{m}_{p,q,s}(\mathtt{D}_h(X) \cap B_R(x+\vec{\delta}), h) &= \hat{m}_{p,q,s}(\mathtt{D}_h(X) \cap B_R(x), h) \\ &+ \hat{m}_{p,q,s}(\mathtt{D}_h(X) \cap (B_R(x+\vec{\delta}) \setminus B_R(x)), h) - \hat{m}_{p,q,s}(\mathtt{D}_h(X) \cap (B_R(x) \setminus B_R(x+\vec{\delta})), h).\end{aligned}$$

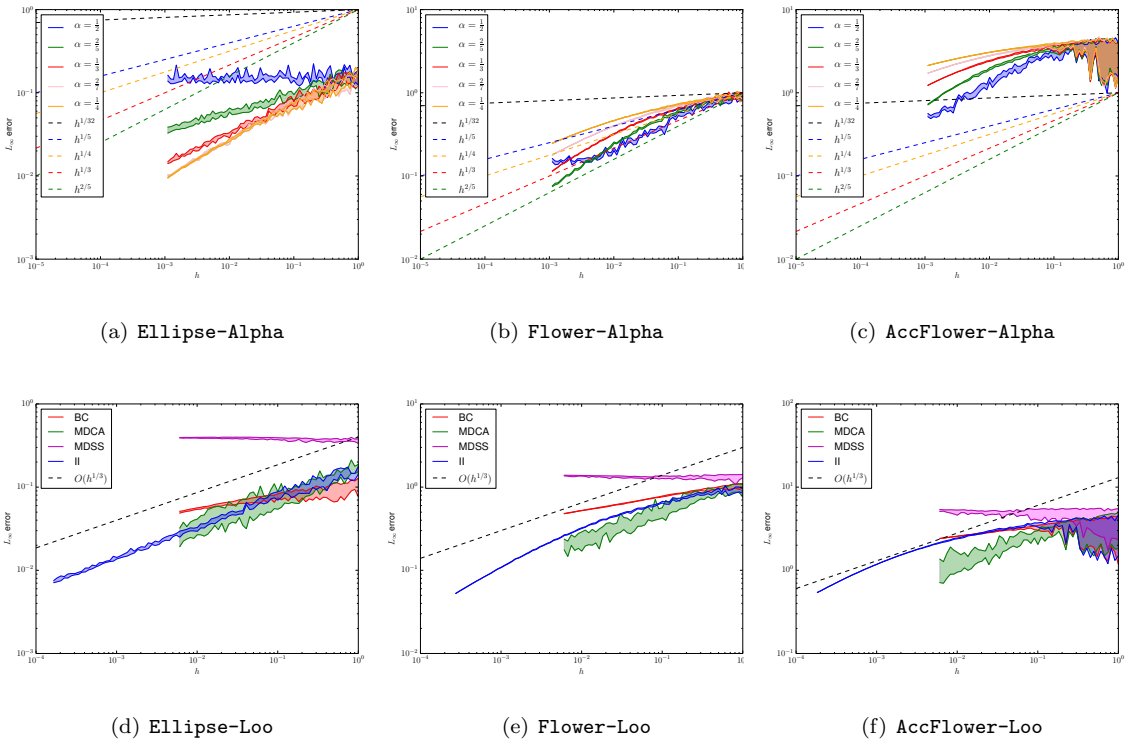

(a) `Ellipse-Alpha` (b) `Flower-Alpha` (c) `AccFlower-Alpha`

(d) `Ellipse-Loo` (e) `Flower-Loo` (f) `AccFlower-Loo`

Figure 2: Exp.

If we precompute all kernels $\mathtt{D}_h(B_R(0 \pm \vec{\delta}) \setminus B_R(0))$ for some $\vec{\delta}$ displacements (based on surface element umbrella configurations, 8 in 2D and 26 in 3D for $\|\vec{\delta}\|_\infty = h$), the computational cost per surface element can be reduced to $O((R/h)^{d-1})$. Finally, on an ideal case the first surfel has to be computed using kernel $B_R(\hat{x})$ and the subsequent neighboring surfels are processed using sub-kernels $\mathtt{D}_h(B_R(0 \pm \vec{\delta}) \setminus B_R(0))$.

As discussed in the previous section, we first validate the experimental multigrid convergence for various α_m parameters. Theorem *article DGCI* says that to obtain at less a uniform convergence of 2d and 3d mean curvature estimators in $Oh^{\frac{1}{3}}$, α_m needs to be equal to 1/3. This α_m will influence the size of the Ball, given by $R = kh^\alpha$. We test five distinct α_m : $\frac{1}{2}$, $\frac{2}{5}$, $\frac{1}{3}$, $\frac{2}{7}$ and $\frac{1}{4}$

We have a collection of multigrid shapes who we know for every points of the *digital border* the exact curvature value. We can easily compute the L_∞ error of our estimator for each α_m. This correspond to the worst-case errors. First in 2d, in Fig. **??** we use an Ellipse which corresponds to theorem hypothesis (convex C^3 shape). We observe convergence for several α_m values. Moreover, the $\frac{1}{3}$ $L_o o$ error behavior is experimentally in $O(h^{\frac{1}{3}})$ as suggested by the theorem. $\alpha_m = \frac{2}{7}$ and $\frac{1}{4}$ provide better worst-case errors because $\frac{1}{3}$ provide a uniform convergence in general case but can be improve with some hypothesis on the shape.

We explore out of the theorem hypothesis scope to observe the behavior on concave shapes as Flower

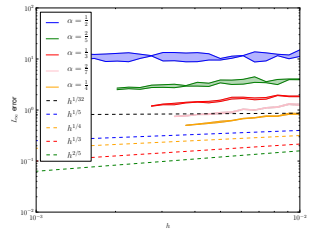

(a) `Sphere-Mean-Alpha`

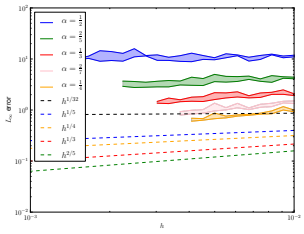

(b) `RoundedCube2-Mean-Alpha`

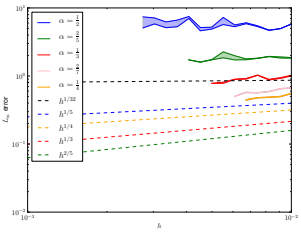

(c) `BlobbyCube-Mean-Alpha`

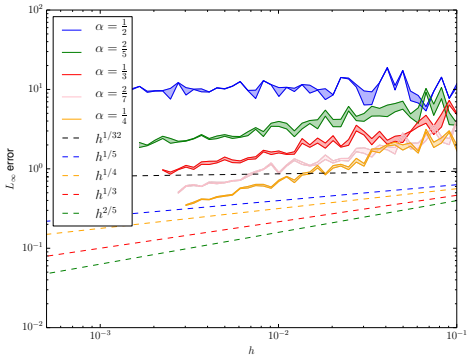

(d) `Sphere-k1-Loo`

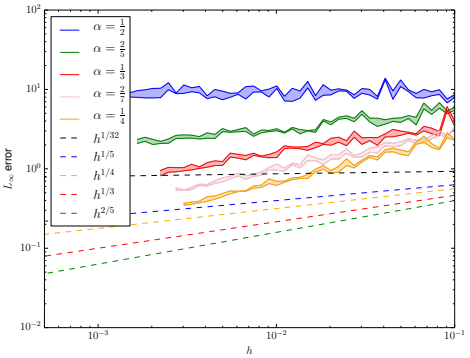

(e) `Sphere-k2-Loo`

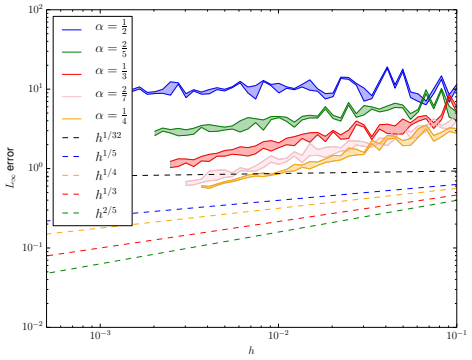

(f) `RoundedCube2-k1-Loo`

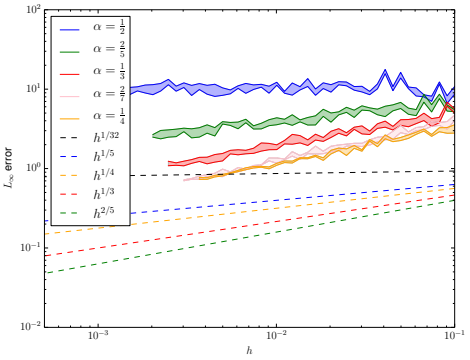

(g) `RoundedCube2-k2-Loo`

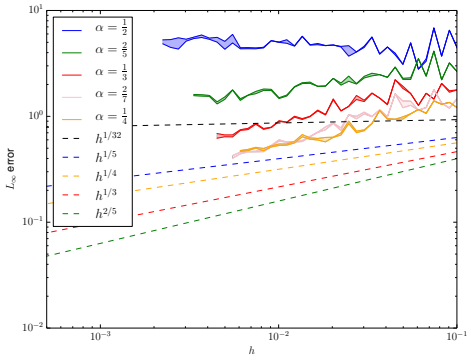

(h) `BlobbyCube-k1-Loo`

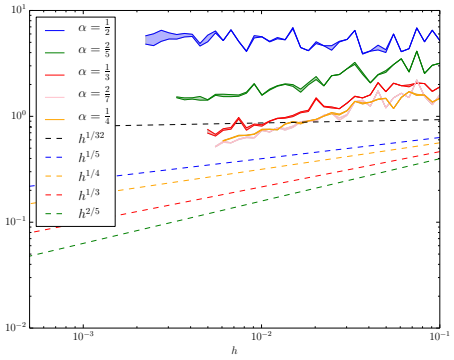

(i) `BlobbyCube-k1-Loo`

Figure 3: Exp.

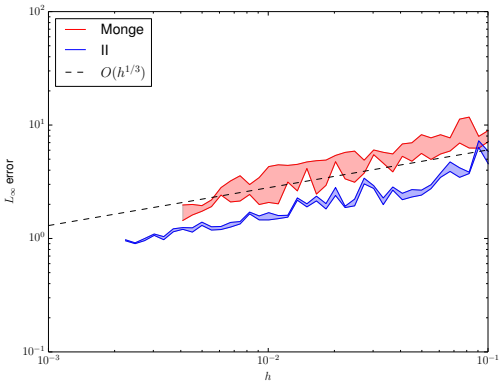

(a) `Sphere-k1-Loo`

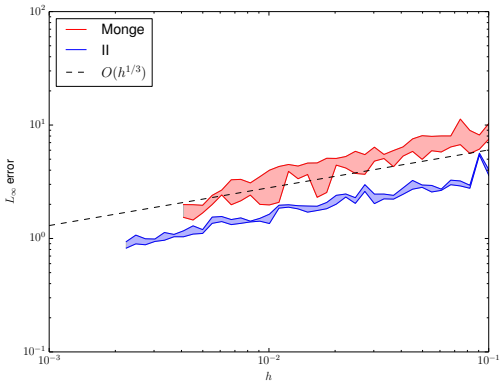

(b) `Sphere-k2-Loo`

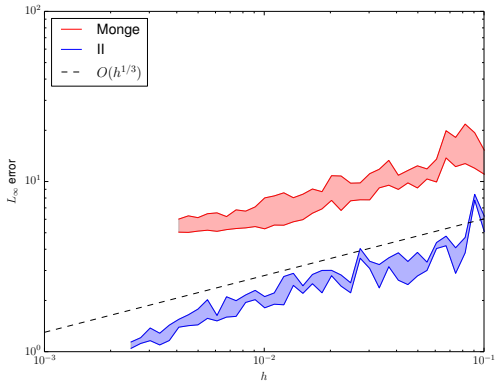

(c) `RoundedCube-k1-Loo`

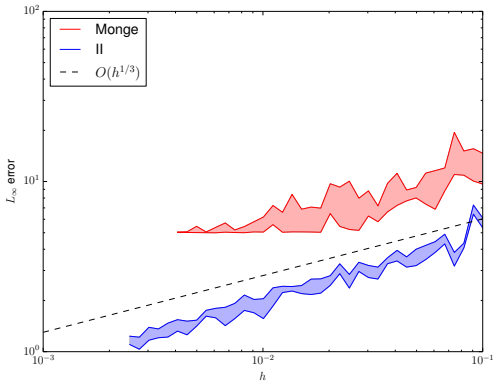

(d) `RoundedCube-k2-Loo`

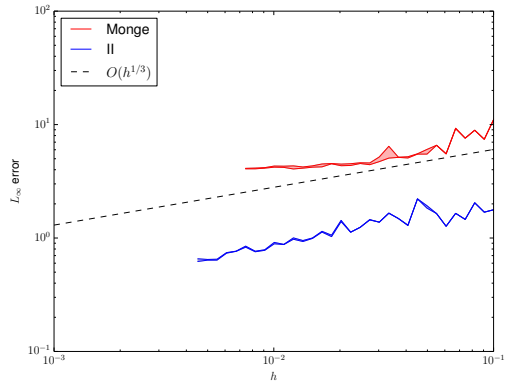

(e) `BlobbyCube-k1-Loo`

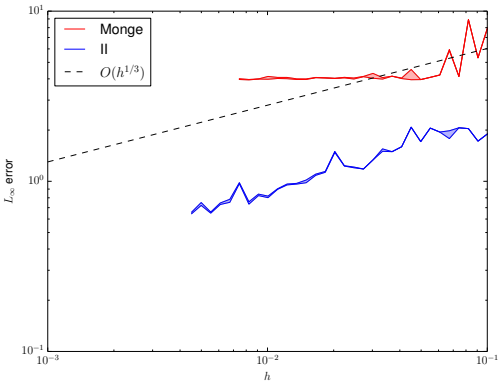

(f) `BlobbyCube-k1-Loo`

Figure 4: Exp.

Fig. ?? and AccFlower Fig. ??. We still observe the convergence but values α_m higher than $\frac{1}{3}$ (and thus larger digital kernel size) seem to lead to lower error values.

In Fig. ??Fig. ??Fig. ??, we compare the proposed 2D curvature estimator (II with $\alpha_m = \frac{1}{3}$) with binomial convolution, MDSS and MDCA estimator for the l_∞ error metric. For more stability of the results, we compute each estimators centered on a random uniform draw location. This is why we have a range of values for estimators. We see that more we going far with the h parameter, more estimators are stable.

In these noise-free object, MDCA performs better or equal than II or Binomial. However, since II and Binomial are based on integration, we may expect better results on noisy objects. MDSS is shown experimentaly non convergent, as expected. Note that in our experiments, observed convergence speeds on ellipses are: *$O(h^{0.154})$ for binomial, $O(h^{0.42})$ for MDCA, and $O(h^{0.38})$ for II* using least square linear fitting. *The first one differs from theoretical results of [25].* In both graphs, we had to stop the computations for Binomial and MDCA for the following reasons: for our implementation of Binomial, the mask size was too large for small h values which induces memory usage issues.

For MDCA, circular arc recognition in `DGtal` is driven by a geometrical predicate based on a determinant computation of squared point coordinates. Hence, small h values lead to numerical capacity issues and thus instability (which could be solved considering arbitrary precision integer numbers but would lead to efficiency issues).

The proposed integral invariant estimator does not suffer from these two kind of issues.

We have performed the same analysis in 3D for the mean curvature: for the validation of the α_m parameter, we compute II with some different α_m values on a rounded cube (convexe, Fig. ?? for mean curvature, Fig. ?? for Gaussian curvature), a blobby cube[6] (concave, Fig. ??, Fig. ??) and a Leopold surface (concave, Fig. ??, Fig. ??). *mettre les formules en bas de page*. We observe on both convexe and concave shapes that $\alpha_m = \frac{1}{3}$ lead to a uniform convergence in $Oh^{\frac{1}{3}}$. *peut etre parler des autres alpha, comme en 2D*

We have compared with Monge (polynomial surface fitting of osculating jets) as described in [?] who provide good results. We see for mean Curvature on rounded cube that II and Monge have the same behavior, better than $Oh^{\frac{1}{3}}$. We also see that for a given h, II provide better results than Monge. With Gaussian curvature, we observe the same thing.

On non-convexe shapes, this is a little different. The asymptotic behavior of Monge is better than II (*donner les pentes pour Blobby*) in both mean and Gaussian.

But an advantage of using II is that it takes less longer to computer for a given h on the digital surface of a shape than Monge Fig. ??.

We also experiment the behavior of the ———————————

Fig. 6, right, details timings for the 2D accelerated flower and for the 3D blobby cube (see below). We

[6]Blobby cube implicit surface is $81x^4 + 81y^4 + 81z^4 - 45x^2 - 45y^2 - 45z^2 - 6 = 0$.

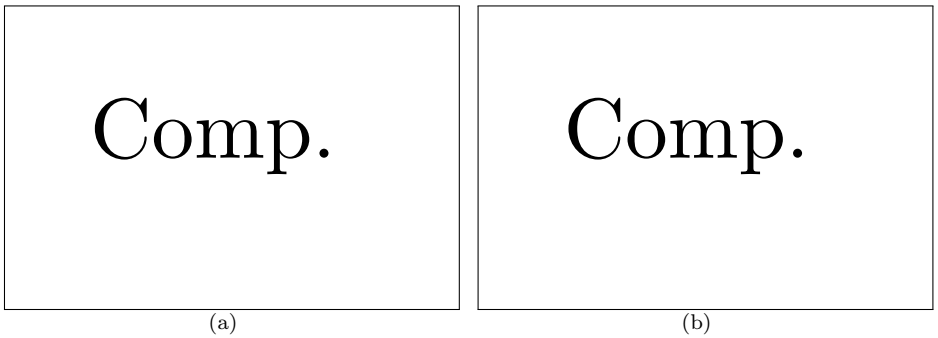

(a) (b)

Figure 5: Comparison of L_∞ error with Binomial [25] and MDCA [27] on multigrid ellipses (left) and accelerated flower (right).

have performed the same analysis in 3D for the mean curvature: evaluation of α_m parameters (Fig. 6, left) on a blobby cube[7]. Concerning the literature and as far as we know, no estimators target multigrid convergence. We have compared with fixed neighborhood convolution as described in [30].

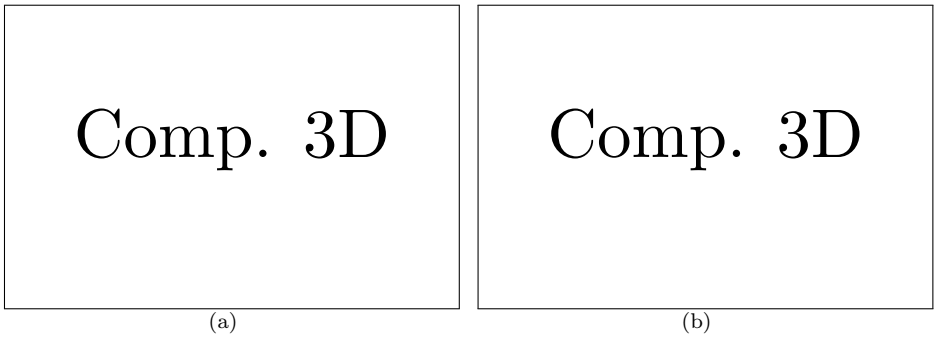

(a) (b)

Figure 6: (Left) Experimental evaluation for mean curvature on blobby cube. (Right) Computational efficiency in dimension 2 (blue, cyan and red) and 3 (black).

Finally, Fig. 7 illustrates mean and Gaussian curvature estimation in 3D (based on covariance matrix of the intersection between the kernel and the shape) and principal curvature directions (eigenvectors of the covariance matrix). Concerning mean curvature, setting $\alpha_m = \frac{1}{3}$ leads to an experimental convergence speed in $O(h^{0.52})$ for the blobby cube, which means either that $h^{\frac{1}{3}}$ is not a tight upper bound or that tested parameters h are not small enough and far from the asymptotic behavior (note that for the finest experiment $h = 0.0247$, the object surface contains 1277288 elements).

5. Conclusion

In this paper, we have used integral invariant results from differential geometry to design simple and efficient digital curvature estimator in dimension 2 and 3. Digital Geometry is a perfect domain for such

[7]Implicit surface is $81x^4 + 81y^4 + 81z^4 - 45x^2 - 45y^2 - 45z^2 - 6 = 0$.

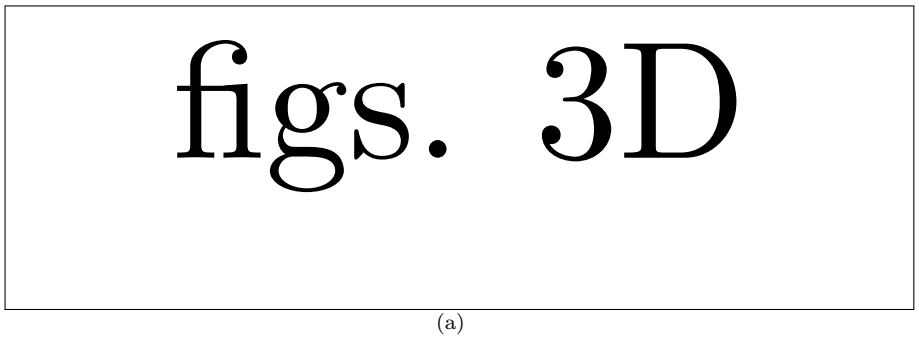

(a)

Figure 7: Illustration of curvature estimation on a 3D blobby cube. *From left to right*: mean curvature and Gaussian curvature mapping ($h = 0.02$, highest is yellow, lowest is blue, red is in-between, furthermore we have set to black zero curvature surfels), first and second principal curvature directions.

differential tools: volume, area or geometrical moments computations are digital by nature, interesting connections to fundamental results on Gauss digitization exist, fast computations induced by the specific geometry of digital surfaces.

For curvature estimation in dimension 2 as well as principal curvature estimations in dimension 3, we have proven a theoretical convergence in $O(h^{\frac{1}{3}})$ for C^3 smooth object boundaries. Evaluation confirms this bound and has demonstrated efficient algorithm in practice with low computational costs. Convergence speed are obtained with a weak constraint on the distance between $\hat{x}$ and x (which just needs to be lower that h for the l_∞ metric). Using specific projection as discussed in [33], better convergence speed is expected at least for dimension 2.

Acknowledgment

This work has been mainly funded by DigitalSnow ANR-11-BS02-009 research grants. We gratefully acknowledge support from the CNRS/IN2P3 Computing Center (Lyon/Villeurbanne - France), for providing a significant amount of the computing resources needed for this work.

Appendix A. Technical lemmas

Appendix A.1. Technical lemmas related to covariance matrices and continuous moments

We gather here a few technical facts and results related to covariance matrices, digital and continuous (p, q, s)-moments.

Lemma 4. *Translation invariance for covariance matrix:*

- *for any finite subset $Y \subset R^3$, for any vector $\mathbf{v} \in \mathbb{R}^3$, $J(Y + \mathbf{v}) = J(Y)$.*

- *for any finite subset $Z \subset Z^3$, for any integral vector $\mathbf{v} \in \mathbb{Z}^3$, for any $h > 0$, $\hat{J}_h(Z + \mathbf{v}) = \hat{J}_h(Z)$.*

Lemma 5. *Let $B_R(t)$ be the ball of radius R and center t. Then, for any non-empty $Y \subset B_R(t)$,*

$$m_{0,0,0}(Y) = O(R^3), \tag{A.1}$$

$$m_{p,q,s}(Y) = O(R^3(\|t\|_\infty + R)), \quad (p+q+s=1) \tag{A.2}$$

$$m_{p,q,s}(Y) = O(R^3(\|t\|_\infty^2 + R\|t\|_\infty + R^2)), \quad (p+q+s=2) \tag{A.3}$$

and

$$m_{p,q,s}(Y)/m_{0,0,0}(Y) = O(R+t), \quad (p+q+s=1) \tag{A.4}$$

Proof. Equ. Eq.(A.1) is immediate since 0-order moment is the volume of Y, hence it cannot exceed the volume of the ball which is $\frac{4}{3}\pi R^3$. For Eq.(A.2), we make the change of variable $(x', y', z') = (x, y, z) - t$ in the following expression:

$$\begin{aligned} m_{1,0,0}(Y) &= \iiint_Y x dx dy dz = \iiint_{Y-t} (x' + t_x) dx' dy' dz' \\ &= t_x \mathrm{Vol}(Y) + m_{1,0,0}(Y - t). \end{aligned}$$

In the first term, $\mathrm{Vol}(Y)$ is bounded by the volume of any ball of radius R. By the additivity of integrals, the second term is maximized by the $(1,0,0)$-moment of the half-ball $B_R^+(0)$ centered on 0 and lying in the positive x orthants. Now, using spherical coordinates, we get

$$\begin{aligned} m_{1,0,0}(B_R^+(0)) &= \int_0^R \int_{\frac{-\pi}{2}}^{\frac{\pi}{2}} \int_{\frac{-\pi}{2}}^{\frac{\pi}{2}} (\rho\cos\phi\cos\theta)(\rho^2\cos\phi)\, d\theta d\phi d\rho \\ &= \left[\frac{\rho^4}{4}\right]_0^R [\sin\theta]_{-\frac{\pi}{2}}^{\frac{\pi}{2}} \frac{1}{2}[\phi + \sin(\phi)\cos(\phi)]_{-\frac{\pi}{2}}^{\frac{\pi}{2}} \\ &= \frac{\pi}{4} R^4, \end{aligned} \tag{A.5}$$

which concludes for Eq.(A.2) (other cases $p+q+s=1$ are similar). Other equations are proved in a similar way.

Appendix A.2. Proof of lemma 3

Proof. By decomposing X according to the two shifted balls (see Fig. A.8), we get:

$$\begin{aligned} m_{p,q,s}(B_R(x+\mathbf{t}) \cap X) - m_{p,q,s}(B_R(x) \cap X) &= m_{p,q,s}((B_R(x+\mathbf{t}) \setminus B_R(x)) \cap X) \\ &\quad - m_{p,q,s}((B_R(x) \setminus B_R(x+\mathbf{t})) \cap X) \end{aligned}$$

We denote by $\Delta(\mathbf{t})$ the difference on the right term of preceding equation. The two sets on the right form the symmetric difference (symbol $\ominus$) of the two shifted balls. We will use the following fact:

$$\emptyset \neq Y_1 \subset Y_2 \subset \mathbb{R}^3 \Rightarrow |\sup_{Y \subset Y_1} m_{p,q,s}(Y)| \leq |\sup_{Y \subset Y_2} m_{p,q,s}(Y)|. \tag{A.6}$$

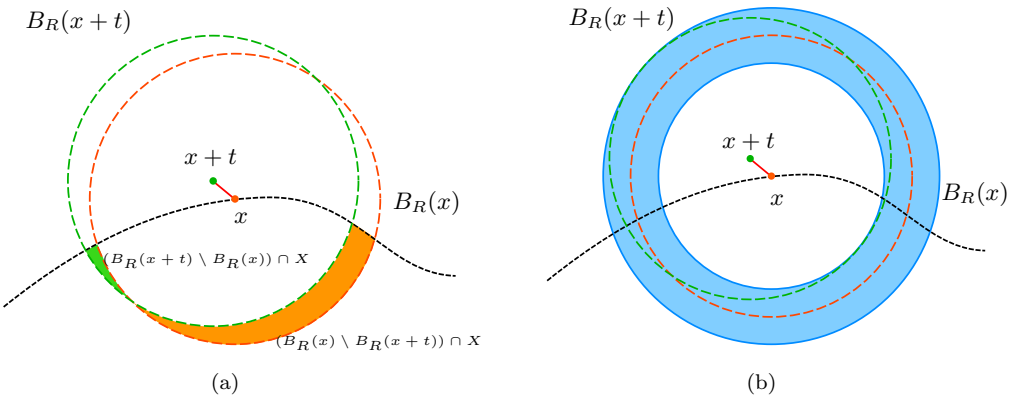

Figure A.8: Illustration for Lemma 3.

By additivity of integrals, we have immediately:

$$\begin{aligned}
|\Delta(\mathbf{t})| &= |m_{p,q,s}((B_R(x+\mathbf{t}) \ominus B_R(x)) \cap X)| \\
&\leq \sup_{Y \subset (B_R(x+\mathbf{t}) \ominus B_R(x)) \cap X} |m_{p,q,s}(Y)| \\
&\leq \sup_{Y \subset B_R(x+\mathbf{t}) \ominus B_R(x)} |m_{p,q,s}(Y)| \\
&\leq \sup_{Y \subset B_{R+t}(x) - B_{R-t}(x)} |m_{p,q,s}(Y)|.
\end{aligned}$$

In the last row, we cover the symmetric difference of two shifted balls by the difference of two balls of same center, a kind of spherical shell or annulus in 2D (see Fig. A.8). Although it is a rough upper bound, it induces the same order of perturbation. We denote this set $B_{R+t}(x) - B_{R-t}(x)$ by $H_{R,t}(x)$.

For zeroth order moment, we use simply the volume of the ball:

$$\begin{aligned}
\sup_{Y \subset H_{R,t}(x)} |m_{0,0,0}(Y)| &= m_{0,0,0}(H_{R,t}(x)) \\
&= \frac{4\pi}{3}(6R^2t + 2t^3) = O(tR^2).
\end{aligned} \tag{A.7}$$

For first order moment, we translate the shape to the origin, then we use the previous result plus the fact that the centered 1,0,0-moment is maximized by the x-positive half-ball:

$$\begin{aligned}
\sup_{Y \subset H_{R,t}(x)} |m_{1,0,0}(Y)| &\leq \sup_{Y \subset H_{R,t}(0)} |m_{1,0,0}(Y)| + |x_x||m_{0,0,0}(Y)| \\
&= m_{1,0,0}(B^+_{R+t}(0) - B^+_{R-t}(0)) + O(|x_x|tR^2) \\
&= 2\pi(R^3t + Rt^3) + O(|x_x|tR^2) \\
&= O(tR^3) + O(\|x\|tR^2).
\end{aligned} \tag{A.8}$$

For second order moment, we translate the shape to the origin, then we use the two previous results plus

the fact that the 2,0,0-moment is maximized by the ball:

$$\begin{aligned}\sup_{Y\subset H_{R,t}(x)}|m_{2,0,0}(Y)| &\leq \sup_{Y\subset H_{R,t}(0)}|m_{2,0,0}(Y)| + 2|x_x||m_{1,0,0}(Y) + x_x^2|m_{0,0,0}(Y)| \\ &= m_{2,0,0}(H_{R,t}(0)) + \|x\|(O(tR^3) + O(\|x\|tR^2)) + x_x^2 O(tR^2) \\ &= O(tR^4) + O(\|x\|tR^3) + O(\|x\|^2 tR^2) \qquad \text{(A.9)}\end{aligned}$$

Other moments are proved similarly. □

References

[1] R. Klette, A. Rosenfeld, Digital Geometry: Geometric Methods for Digital Picture Analysis, Series in Computer Graphics and Geometric Modelin, Morgan Kaufmann, 2004.

[2] D. Coeurjolly, J.-O. Lachaud, T. Roussillon, Digital Geometry Algorithms, Theoretical Foundations and Applications of Computational Imaging, volume 2 of *LNCVB*, Springer, 2012, pp. 395–424.

[3] N. Amenta, M. Bern, M. Kamvysselis, A new voronoi-based surface reconstruction algorithm, in: Proceedings of the 25th annual conference on Computer graphics and interactive techniques, ACM, 1998, pp. 415–421.

[4] Q. Mérigot, M. Ovsjanikov, L. Guibas, Voronoi-based curvature and feature estimation from point clouds, Visualization and Computer Graphics, IEEE Transactions on 17 (2011) 743–756.

[5] T. Surazhsky, E. Magid, O. Soldea, G. Elber, E. Rivlin, A comparison of gaussian and mean curvatures estimation methods on triangular meshes, in: Robotics and Automation, 2003. Proceedings. ICRA '03. IEEE International Conference on, volume 1, 2003, pp. 1021–1026.

[6] T. D. Gatzke, C. M. Grimm, Estimating curvature on triangular meshes, International Journal of Shape Modeling 12 (2006) 1–28.

[7] M. Desbrun, A. N. Hirani, M. Leok, J. E. Marsden, Discrete exterior calculus, arXiv preprint math/0508341 (2005).

[8] A. I. Bobenko, Y. B. Suris, Discrete differential geometry: Integrable structure, volume 98, AMS Bookstore, 2008.

[9] D. L. Page, Y. Sun, A. F. Koschan, J. Paik, M. A. Abidi, Normal vector voting: Crease detection and curvature estimation on large, noisy meshes, Graphical Models 64 (2002) 199–229.

[10] S. Rusinkiewicz, Estimating curvatures and their derivatives on triangle meshes, in: 3D Data Processing, Visualization and Transmission, 2004. 3DPVT 2004. Proceedings. 2nd International Symposium on, 2004, pp. 486–493.

[11] G. Xu, Convergence analysis of a discretization scheme for gaussian curvature over triangular surfaces, Computer Aided Geometric Design 23 (2006) 193–207.

[12] D. Cohen-Steiner, J.-M. Morvan, Restricted delaunay triangulations and normal cycle, in: Proceedings of the nineteenth annual symposium on Computational geometry, SCG'03, ACM, New York, NY, USA, 2003, pp. 312–321. URL: `http://doi.acm.org/10.1145/777792.777839`.

[13] D. Cohen-Steiner, J.-M. Morvan, Second fundamental measure of geometric sets and local approximation of curvatures, Journal of Differential Geometry 74 (2006) 363–394.

[14] H. Pottmann, J. Wallner, Y. Yang, Y. Lai, S. Hu, Principal curvatures from the integral invariant viewpoint, Computer Aided Geometric Design 24 (2007) 428–442.

[15] H. Pottmann, J. Wallner, Q. Huang, Y. Yang, Integral invariants for robust geometry processing, Computer Aided Geometric Design 26 (2009) 37–60.

[16] F. Cazals, M. Pouget, Estimating differential quantities using polynomial fitting of osculating jets, Computer Aided Geometric Design 22 (2005) 121–146.

[17] P. Alliez, D. Cohen-Steiner, Y. Tong, M. Desbrun, Voronoi-based variational reconstruction of unoriented point sets, in: Symposium on Geometry processing, volume 7, 2007, pp. 39–48.

[18] Q. Mérigot, M. Ovsjanikov, L. Guibas, Robust voronoi-based curvature and feature estimation, in: 2009 SIAM/ACM Joint Conference on Geometric and Physical Modeling, SPM'09, ACM, New York, NY, USA, 2009, pp. 1–12. URL: http://doi.acm.org/10.1145/1629255.1629257.

[19] B. Li, R. Schnabel, R. Klein, Z. Cheng, G. Dang, S. Jin, Robust normal estimation for point clouds with sharp features, Computers & Graphics 34 (2010) 94–106.

[20] A. Boulch, R. Marlet, Fast and robust normal estimation for point clouds with sharp features, Computer Graphics Forum 31 (2012) 1765–1774.

[21] J. Zhang, J. Cao, X. Liu, J. Wang, J. Liu, X. Shi, Point cloud normal estimation via low-rank subspace clustering, Computers & Graphics 37 (2013) 697–706.

[22] D. Coeurjolly, R. Klette, A comparative evaluation of length estimators of digital curves, IEEE Trans. on Pattern Analysis and Machine Intelligence 26 (2004) 252–258.

[23] F. de Vieilleville, J.-O. Lachaud, F. Feschet, Maximal digital straight segments and convergence of discrete geometric estimators, Journal of Mathematical Image and Vision 27 (2007) 471–502.

[24] R. Malgouyres, F. Brunet, S. Fourey, Binomial convolutions and derivatives estimation from noisy discretizations, in: Discrete Geometry for Computer Imagery, volume 4992 of *LNCS*, Springer, 2008, pp. 370–379.

[25] H.-A. Esbelin, R. Malgouyres, C. Cartade, Convergence of binomial-based derivative estimation for 2 noisy discretized curves, Theoretical Computer Science 412 (2011) 4805 – 4813.

[26] L. Provot, Y. Gérard, Estimation of the derivatives of a digital function with a convergent bounded error, in: Discrete Geometry for Computer Imagery, LNCS, Springer, 2011, pp. 284–295.

[27] T. Roussillon, J.-O. Lachaud, Accurate curvature estimation along digital contours with maximal digital circular arcs, in: Combinatorial Image Analysis, volume 6636, Springer, 2011, pp. 43–55.

[28] B. Kerautret, J.-O. Lachaud, Curvature estimation along noisy digital contours by approximate global optimization, Pattern Recognition 42 (2009) 2265 – 2278.

[29] A. Lenoir, Fast estimation of mean curvature on the surface of a 3d discrete object, in: E. Ahronovitz, C. Fiorio (Eds.), Proc. Discrete Geometry for Computer Imagery (DGCI'97), volume 1347 of *Lecture Notes in Computer Science*, Springer Berlin Heidelberg, 1997, pp. 175–186. URL: http://dx.doi.org/10.1007/BFb0024839.

[30] S. Fourey, R. Malgouyres, Normals and curvature estimation for digital surfaces based on convolutions, in: Discrete Geometry for Computer Imagery, LNCS, Springer, 2008, pp. 287–298.

[31] D. Coeurjolly, J. L. Lachaud, J. Levallois, Integral based curvature estimators in digital geometry, in: Discrete Geometry for Computer Imagery, number 7749 in LNCS, Springer, 2013, pp. 215–227.

[32] DGtal: Digital geometry tools and algorithms library, ???? http://libdgtal.org.

[33] J.-O. Lachaud, Espaces non-euclidiens et analyse d'image : modèles déformables riemanniens et discrets, topologie et géométrie discrète, Habilitation à diriger des recherches, Université Bordeaux 1, Talence, France, 2006.

[34] J. W. Bullard, E. J. Garboczi, W. C. Carter, E. R. Fullet, Numerical methods for computing interfacial mean curvature, Computational materials science 4 (1995) 103–116.

[35] E. Krätzel, Lattice points, volume 33, Springer, 1988.

[36] M. N. Huxley, Area, lattice points and exponential sums, Oxford Science publications, 1996.

[37] R. Klette, J. Žunić, Multigrid convergence of calculated features in image analysis, Journal of Mathematical Imaging and Vision 13 (2000) 173–191.

[38] E. Krätzel, W. G. Nowak, Lattice points in large convex bodies, Monatshefte für Mathematik 112 (1991) 61–72.

[39] W. Müller, Lattice points in large convex bodies, Monatshefte für Mathematik 128 (1999) 315–330.

[40] G. W. Stewart, J.-g. Sun, Matrix perturbation theory (1990).

[41] R. Bhatia, Matrix analysis, volume 169, Springer, 1997.